Available online at www.sciencedirect.com

ScienceDirect

Procedia Engineering 10 (2011) 2298–2311

Engineering Procedia

ICM11

Damage and energy absorption in GFRP laminates impacted at low-velocity: indentation model

G. Caprino, V. Lopresto*, A. Langella, C. Leone

Department of Materials and Production Engineering, University of Naples "Federico II", Piazzale Tecchio, 80, 80125, Naples, Italy

Abstract

Low-velocity impact tests were carried out on glass-fibre-reinforced plastic panels, varying the impact energy, laminate thickness, and tup diameter. A previous model, aimed at the prediction of indentation as a function of impact energy, was slightly modified, to establish a correlation of the dent depth with absorbed energy. Good agreement was found between the theoretical predictions and experimental results. Further, the possibility to resort to the absorbed energy from an indentation measurement, using a single curve valid whichever the laminate thickness and impactor diameter, was demonstrated. Analyzing previous experimental data, concerning carbon-fibre-reinforced plastics, the different behaviour of GFRP and CFRP in absorbing energy and undergoing indentation was revealed. New results about basalt fibre laminates based on a limited number of experimental tests were reported too.

Keywords: Polymer-matrix composites; Impact behaviour; Mechanical testing; Indentation.

1. Introduction

In the last decades, many researchers have studied the response of composite materials to impact, identifying the damage mechanisms occurring in the material [1,2], as well as their effect on residual properties [3,4]. Despite the experimental and analytical efforts, many questions remain to be answered. The complex interaction between the failure modes, influenced by a variety of parameters such as fibre and matrix type, reinforcement architecture, and constraint conditions, cannot be easily predicted by analytical and numerical tools. The same holds for residual compression strength after impact, one of the most important factors affecting design allowable.

* Corresponding author. V. Lopresto, Tel.: +39 081 76822216; fax: +39 081 7682362.
E-mail address: lopresto@unina.it.

 doi:10.1016/j.proeng.2011.04.380

Another topic quite obscure at this time is the way through which the initial energy of the projectile is introduced into the target. In a non-perforating impact, a part of this energy is stored elastically, resulting in tup rebound, and can be easily measured. On the contrary, it is hard to share the absorbed energy, which is partially dissipated under form of heat and vibrations, but also contributes to damage development, determining fibre breakage, delamination, intralaminar splitting, permanent indentation and fractures at the fibre-matrix interface.

Recognizing the relative importance of the different phenomena taking place the energy absorption plays a fundamental role in the development of composite materials with improved impact resistance and tolerance. Some contribution to this topic has been given, among others, by Sutherland and Guedes Soares [5] and Delfosse and Poursartip [6]. The former authors demonstrated that the evolution of absorbed energy with increasing impact energy could reveal first fibre fracture; the latter attempted to quantify the relationship between the damage mechanisms and energy absorption, as a function of projectile displacement and impact energy. Since the analysis of absorbed energy seems to be the key point to better understand impact damage, this work had two main objectives: a) to verify whether the absorbed energy could be inferred from an indentation measurement; b) to assess the model proposed by Delfosse and Poursartip [6], derived from energy balance considerations, characterizing the internal damage by appropriate observation of the failure modes. The low-velocity impact tests were carried out on Glass-Fibre-Reinforced Plastic (GFRP) laminates, varying both the panel thickness and the impactor diameter.

The variation of the absorbed energy with increasing impact energy is discussed, and a previous model [7] is modified, with the scope of correlating the absorbed energy and dent depth. A comparison with Carbon Fibre Reinforced Plastic (CFRP) laminates data from literature was proposed too. Just to give a first general idea about the impact behaviour of a material very limited in application at today but very promising in performances [8], a limited number of experimental low velocity impact tests were carried out also on basalt fibre laminates.

2. Indentation law

In studying the problem of low-velocity impact on Carbon-Fibre-Reinforced Plastic (CFRP) laminates, Caprino and co-workers [7] proposed the following empirical formula:

$$I = k' \cdot [10^{\gamma'(U/Up)} - 1] \tag{1}$$

correlating the impact energy, U, with indentation, I, through the constants k' and γ', to be experimentally determined. In Eq. (1), U_p is the perforation energy, which of course depends on the laminate thickness and indenter diameter, increasing with them.

The data presented and discussed [7] showed that k' and γ' are conceivably dependent on the fibre type under concern, being insensitive to the panel thickness and constraint conditions, reinforcement architecture, orientation of the layers in the laminate, and matrix type.

In this work, the following modified indentation model will be assessed:

$$I = k \cdot [10^{\gamma'(U_a/Up)} - 1] \tag{2}$$

Eq. (2) is formally identical to Eq. (1), except for the impact energy U, which is substituted by the absorbed energy U_a, i.e. the energy not transferred back to the rebounding tup in a non-perforating impact.

In principle, Eq. (2) is physically more consistent than Eq. (1), predicting no indentation, unless some energy is lost by the projectile during impact.

To evaluate the constants appearing in Eq. (2), the relationship can be expressed in the following form:

$$Log(\frac{I}{k}+1) = \gamma \cdot \frac{U_a}{U_p} \quad (3)$$

from which, plotting the term on the left against the non-dimensional absorbed energy would result in a straight line passing through the origin, having slope γ. Therefore, a trial-and-error procedure can be used to calculate the material constants, varying k until the straight line best fitting the data in the diagram $Log(I/k+1)$-U_a/U_p will pass through the origin. This method was successfully adopted in [7].

3. Materials and test methods

The laminates examined in this work were obtained from GFRP prepreg made of plain-wave E-glass fabric 295 g/m^2 in areal weight and Cycom 7701 epoxy resin. Square panels 330 mm in side were fabricated by hand lay-up and cured under press for 2 hours at 120°C temperature and 0.1 MPa pressure. The stacking sequence adopted was $[(0,90)_n/(+45,-45)_n/(+45,-45)_n/(0,90)_n]$, with n=1 to 4. The final thickness was (0.96n) mm, and the fibre content by volume V_f=0.47.

Basalt fibre reinforced plastic laminates with 300 mm x 300 mm in plane dimensions were obtained through infusion technology. The different types of reinforcement employed were: basalt dry fabrics, 200 g/m2, plain-weave (warp 10F/10 mm, weft 10F/10 mm), tex 100, from ZLBM (De). In order to produce plates with the desired thickness, a sufficient number of plies were overlapped on a release film placed on a glass tool. Then, they were covered with the peel ply and the plastic bag. After that, the preforms were impregnated through resin infusion by an epoxy matrix (Becor I-SX10 + hardener SX10M). The curing stage at room temperature and at a vacuum level of -990 mbar was performed for 24 hours. The following stacking sequence was obtained: $[(0,90)/(+45,-45)/(+45,-45)/(0,90)]_n$, with n=2 to 4, leading to nominal thickness of 1, 2 and 3 mm and a fibre volume fraction V_f = 50%. From the plates, square specimens 70 mm in side, destined to impact, were cut by a diamond saw.

The low-velocity impact tests were carried out in a Ceast MK4 instrumented testing machine, equipped with a DAS 4000 digital acquisition system. The samples were simply supported on a steel plate with a circular opening 50 mm in diameter, and struck at the centre using two hemispherical steel tups, 16 mm and 19.8 mm in diameter, D_t, respectively for the glass fibre laminates whereas only the last one was used for the basalt ones. To prevent multiple impacts, the tup was caught on the rebound by a brake available in the test apparatus.

A first series of tests, aiming to obtain the Force-displacement (F-d) curve up to perforation, was carried out using a mass M=10.6 Kg falling from 1 m height. From the F-d curves recorded for each panel thickness, four characteristic energy levels were selected, and reproduced in the subsequent impact tests, which will be designated as “indentation tests” hereafter. In these tests, the energy was set by suitably combining the falling eight and three masses (M=3.6, 5.6, 7.6 Kg) available in the testing machine. In all, at least three impact tests were performed for each experimental condition.

After impact, indentation was evaluated according to EN 6038 standard.

4. Results and discussion

4.1. Impact curves

Typical impact curves recorded during the perforation tests, illustrating the effect of panel thickness, are collected in Fig. 1. They are all about glass fibre laminates but the same characteristics were confirmed by carbon and basalt laminates load curves.

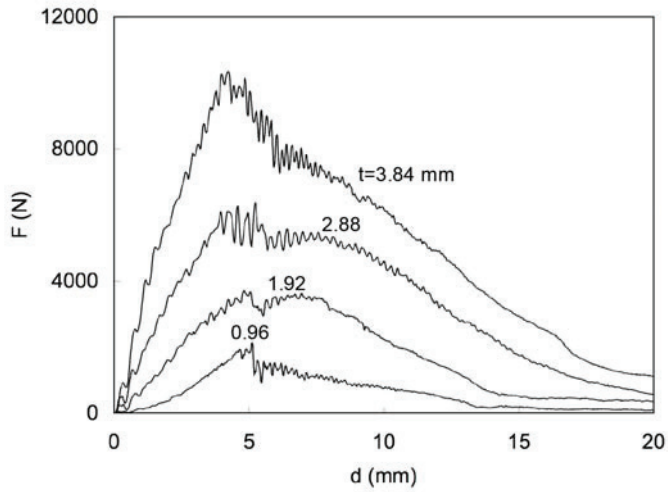

Fig.1. Typical force-displacement curves recorded during the perforation tests for the different panel thicknesses t tested. Impactor diameter D_t=19.8 mm. Material: GFRP.

As usually found, for a fixed displacement, an increase in t results in a clear increase in the contact force. The effect of t on the displacement range over which the entire contact history occurs is far smaller.

Irrespective of t and D_t, all the F-d curves reveal common features. At low displacement, the material behaviour is elastic, and disturbed by dynamic oscillations the more marked, the thicker the panel is. At a sufficiently high load, a sequence of sudden load drops, indicating significant failure [9], appears, with the general trend of the contact force increasing yet. Around the peak load, dramatic load drops, suggesting major damage, are observed, with the F-d curve flattening out. Finally, the force begins to smoothly decrease, until the perforation process is completed.

The influence of the tup diameter on the overall trend of the F-d curve is shown in Fig. 2. As expected from heuristic considerations, a smaller tup diameter results in lower contact forces at a given displacement. However, the general shape of the curve previously depicted is preserved.

A more detailed description of the elastic behaviour of the present materials can be found in [9], to which the interested reader can refer. For the scopes of this work, it is useful to recall the energy level U_f in correspondence of which the first sudden load drop, interpreted as first fibre failure [9], was detected. The U_f values are collected in Tab. I, together with the perforation energies U_p, measured for each panel thickness from the complete F-d curves.

As previously specified, the four energy levels to adopt in the indentation tests were defined from the observation of the complete F-d curves. In particular, the first energy level was slightly in excess of the energy for first fibre failure, whereas the second and the third corresponded to the portion of the F-d curve

near, but beyond, the peak load. The fourth energy level was associated with the last part of the curve, characterized by a gradual decrease of the contact force.

In Fig. 3, different F-d curves, deriving from impact tests performed with different energies, are superposed. The superposition is good, indicating that, although the energy was varied acting on both the mass and the falling height (i.e. the velocity), the effect of these parameters on the contact history is negligible. Due to this, to designate the different tests, reference will be made uniquely to energy in what follows. In doing this, it will be implicitly assumed that also the failure modes are uniquely affected by energy.

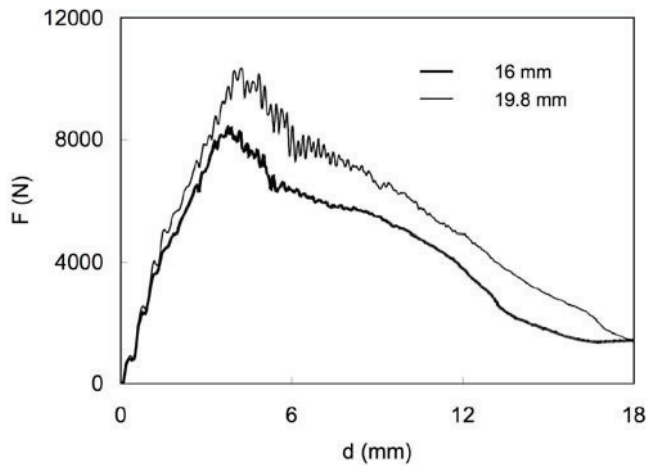

Fig. 2. Effect of the tup diameter, D_t, on the trend of the force-displacement curves. Panel thickness t=3.84 mm. Material: GFRP.

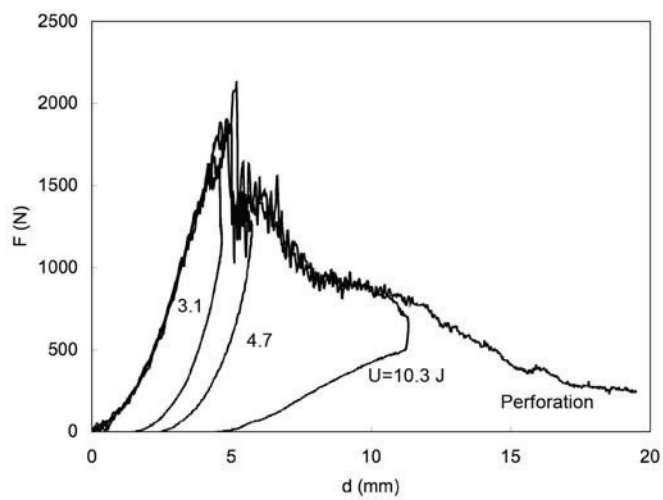

Fig. 3. Typical force-displacement curves recorded during the tests at increasing energy levels, U. Panel thickness t=0.96 mm. Impactor diameter D_t=19.8 mm. Material: GFRP.

Table 1. Energy at first fibre failure, U_f, perforation energy, U_p, for the thicknesses t tested. D_t= impactor diameter. Material: GFRP.

	D_t=16 mm		D_t=19.8 mm	
t (mm)	**U_f (J)**	**U_p (J)**	**U_f (J)**	**U_p (J)**
0.96	0.99	9.3	1.16	13.3
1.92	2.21	22.5	2.50	32.2
2.88	4.26	52.0	4.87	59.5
3.84	7.79	78.6	11.3	98.0

4.2. Absorbed energy

As usual, the absorbed energy was evaluated from the area enclosed within the loading-unloading F-d curves recorded during non-perforating impact tests. Indeed, a very simple equation was found, correlating the impact energy and U_a through the perforation energy. This is shown in Fig. 4, where the nondimensional values of U_a, U_a /U_p, are plotted against the ratio U/U_p for GFRP. In the figure, the vertical bars denote standard deviation, and the different symbols are identified by the label "A/B", where A is the tup diameter and B the panel thickness (in mm).

Clearly, all the data, irrespective of the panel thickness and impactor diameter, collapse into a single, sensibly linear trend. Only at very low non-dimensional impact energies (two extreme points on the left), some deviation from linearity is guessed, with the experimental points approaching origin.

A qualitatively similar correlation between U and U_a was found by Sutherland and Guedes Soares [5]. The authors carried out low-velocity impact tests on GFRP laminates made of different woven roving architectures, thicknesses, and resins. When the absorbed energy was plotted against U, a bi-linear trend was observed, with the knee corresponding to the onset of fibre damage. Accepting this interpretation, the knee in the present case, according to the data in Tab. I, should be located in the range U/U_p=0.08 to 0.11.

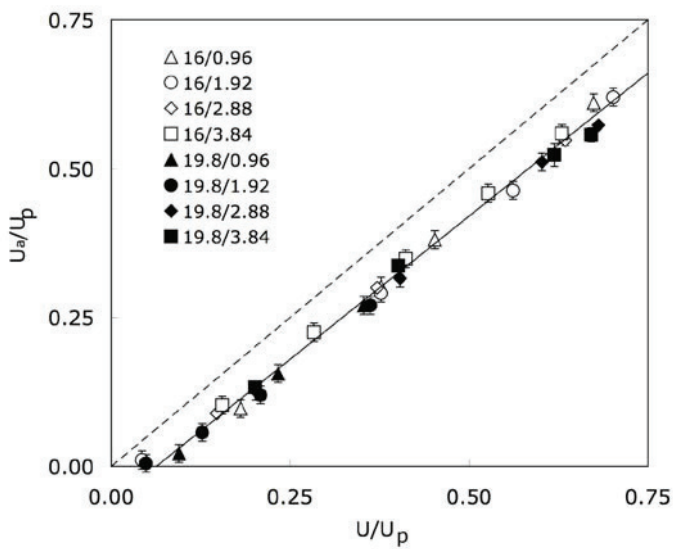

Fig. 4. Non dimensional absorbed energy, U_a/U_p, against non dimensional impact energy, U/U_p.

Discarding the two extreme point on the left in Fig. 4, the solid best-fit straight line, having equation:

$$\frac{U_a}{U_p} = 0.962\frac{U}{U_p} - 0.0609 \tag{4}$$

was obtained. From the results, both the constants in Eq. (4) substantially hold whichever t and D_t. The virtual non-dimensional energy U_o/U_p resulting in $U_a/U_p=0$, graphically represented by the intercept of the straight line with the x-axis, was calculated, giving $U_o/U_p=0.063$. Therefore, would the linear relationship hold also at very low energies, a perfectly elastic impact should occur when the initial energy is 6.3% of the perforation energy, or lower.

The dashed line in Fig. 4 has equation $U_a/U_p= U/U_p$, representing the condition for which all the available energy is absorbed. Since the elastically stored portion of the non-dimensional impact energy, U_{el}/U_p, is given by $U_{el}/U_p = (U- U_a)/U_p$, the vertical distance of the generic experimental point from this line is U_{el}/U_p. With this in mind, and considering that the slope of the continuous line is 0.962, it is concluded that, beyond U_o, the elastic energy negligibly increases with increasing impact energy. Of course, at perforation U_e is nil. It is inferred that, when perforation is approached, the linear relationship highlighted in Fig. 4 will be violated.

The results in Fig. 4 have been rearranged in Fig. 5, plotting U_a/U against U/U_p. The solid line graphically represents the relationship:

$$\frac{U_a}{U} = 0.962 - 0.0609\frac{U_p}{U} \tag{5}$$

which is obtained immediately from Eq. (4).

From Fig. 5, at very low energy a considerable portion of the impact energy is transferred back to the tup. With increasing U, a part lower and lower of the initial energy is stored elastically, compared to the absorbed energy. Even when U is 25% of the perforation energy, about 71% of it is absorbed; for $U/U_p=0.75$, only 12% of the energy is employed for rebound.

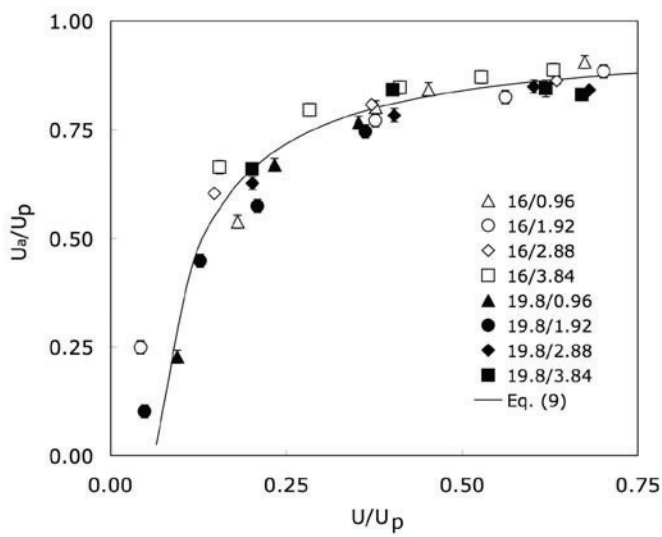

Fig. 5. Non dimensional absorbed energy, U_a/U, against non dimensional impact energy, U/U_p.

4.3. Assessment of the indentation model

In Fig. 6, the measured indentation, I, on GFRP laminates, is shown against impact energy, U. The curves are second-order polynomials, drawn to better illustrate the experimental trends.

Of course, for a given energy, the dent depth is the larger, the thinner is the panel and lower the impactor diameter. Further, as natural, I increases monotonically with increasing U.

As stated previously, Eq. (3) was used to assess the indentation model, plotting all the experimental data on a $\mathrm{Log}(I/k+1).U_a/U_p$ diagram, and varying k until the best-fit straight line passed through the origin. This condition was met for k=1.06 mm, and is represented by the solid line in Fig. 7, whose slope yielded γ=0.931.

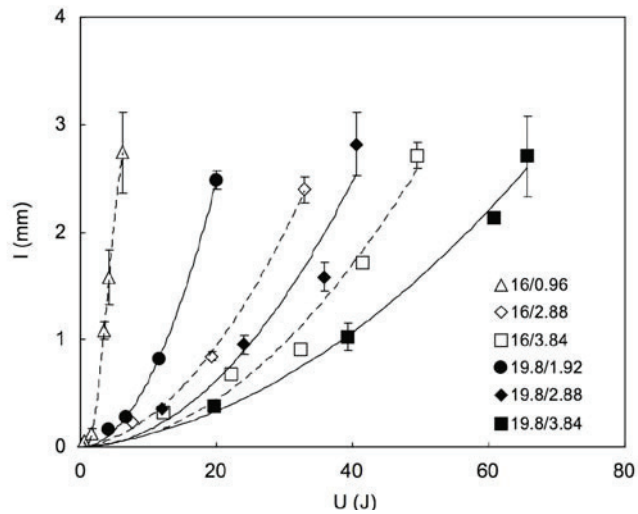

Fig. 6. Indentation, I, against impact energy, U.

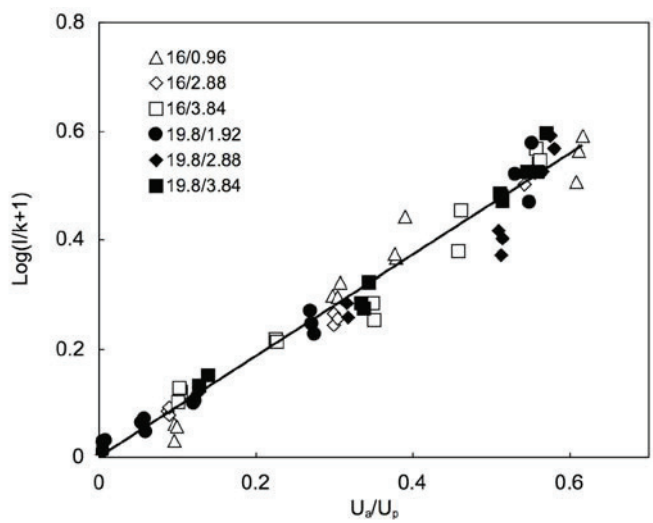

Fig. 7. Diagram for the assessment of the indentation model.

From Fig. 7, both the solid and the open symbols follow with good accuracy the straight line. Consequently, k and γ are insensitive to the panel thickness and tup diameter. The effectiveness of Eq. (2) is better appreciated from Fig. 8, where the model was used to draw the dashed and continuous curves, referring to D_t=16 mm and D_t=19.8 mm, respectively.

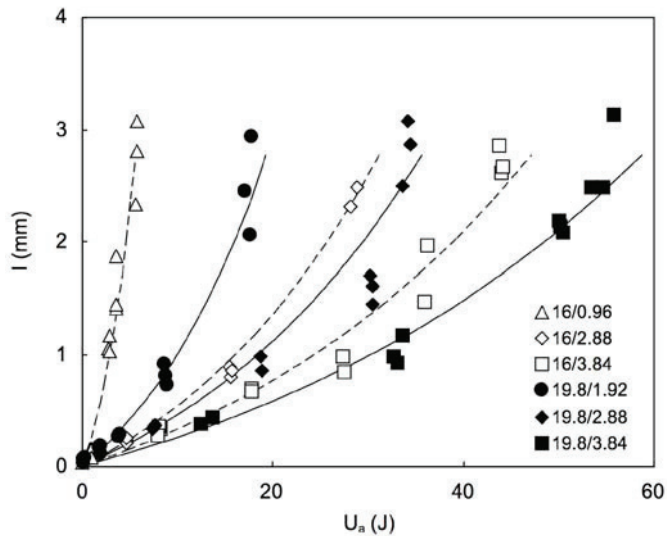

Fig. 8. Indentation, I, against absorbed energy, U_a.

4.3. Comparison with CFRP laminates

In a previous paper [10], the results of low-velocity impact tests carried out on CFRP T400/HMF 934 fabric laminates were presented and discussed. The stacking sequence was $\{[(0, 90)/(\pm 45)]_s\}_n$, with n=1 to 4, and the thicknesses ranged between 0.76 and 3.01 mm. The hemispherical tup diameter was 12.7 mm. Some of the F-d curves recorded in [10] were analyzed anew in this work, the absorbed energy was evaluated, and its non-dimensional value U_a/U_p was plotted against U/U_p (Fig. 9).

From Fig. 9, the bi-linear trend highlighted by Sutherland and Guedes Soares [5], qualitatively depicted by the full line drawn by hand, clearly appears. According to the interpretation given in [5], the onset of fibre damage would occur for $U \sim 0.2U_p$. As discussed previously, the same phenomenon would take place much earlier for the GFRP studied in this work. Another interesting feature of CFRP in Fig. 9 is the fact that the straight line fitting the data located beyond the knee seems to pass through the point (1,1). This suggests that the linear trend is preserved until perforation is accomplished.

Similarly to Fig. 7, Fig. 10 shows the $\mathrm{Log}(I/k+1)$-U_a/U_p diagram for CFRP. Considering the small number of data available, the superposition of the points associated with different thicknesses is reasonably good. From the data, the values k=0.221 mm, γ=1.68 were obtained, and used to predict indentation (continuous curves in Fig. 11).

The previous concepts have been applied in Fig. 12, where all the indentation data concerning GFRP and CFRP are collected. To avoid confusion, in the figure two symbols, only allowing for the distinction between GFRP (open triangles) and CFRP (full circles), have been used.

Despite the scatter affecting the experimental data, the different behaviour of the two material systems is obvious, with GFRP exhibiting a larger indentation, for a fixed value of the non-dimensional absorbed

energy. It is concluded that, when the same indentation is measured on GFRP and CFRP, the latter material absorbs a higher portion of energy, if the perforation energy is assumed as a benchmark.

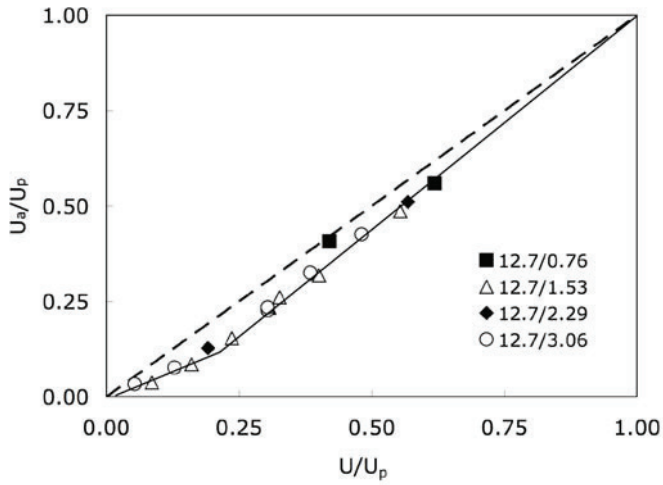

Fig. 9. Non dimensional absorbed energy, U_a/U_p, against non dimensional impact energy, U/U_p. Material: CFRP [10].

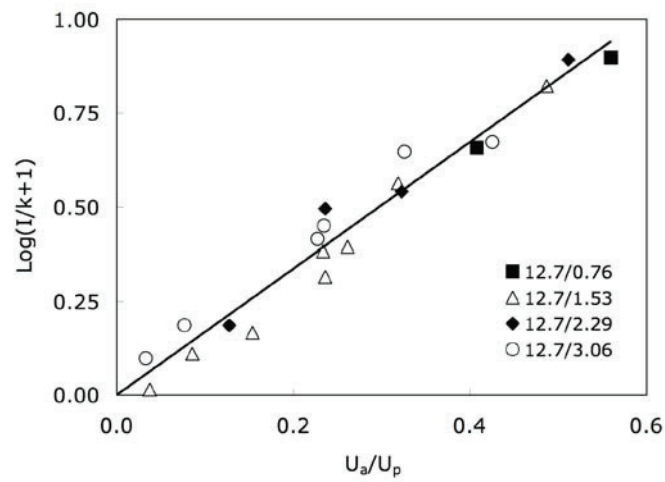

Fig. 10. Diagram for the assessment of the indentation model. Material: CFRP [10].

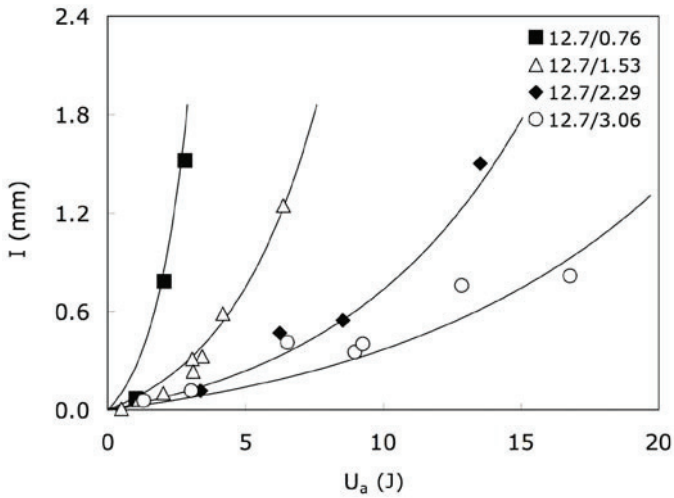

Fig. 11. Indentation, I, against absorbed energy, U_a. Material: CFRP [10].

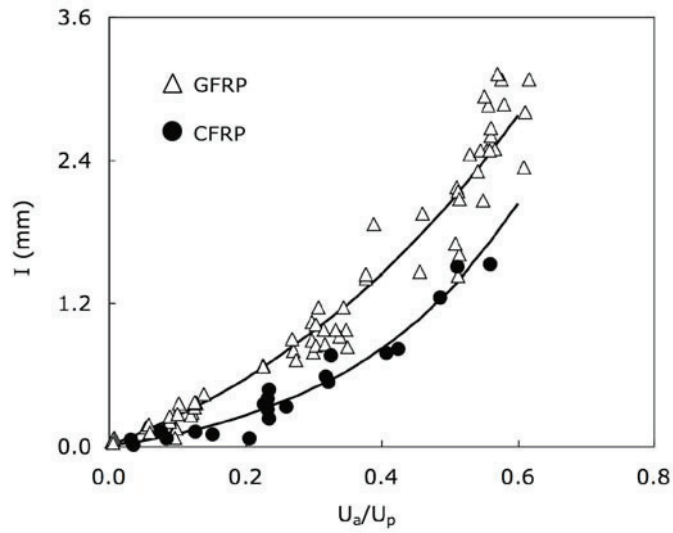

Fig. 12. Indentation, I, against non-dimensional absorbed energy, U_a/U_p, for GFRP (open triangle) and CFPR (full circle).

4.4. Comparison with BFRP laminates

As anticipated, a limited number of low velocity impact tests were carried out on basalt fibre reinforced plastic laminates, BFRP, and the results in terms of indentation and absorbed energy are reported here. The measured non-dimensional value U_a/U_p was plotted against U/U_p (Fig. 13).

Also in Fig. 13 it could be possible to distinguish the bi-linear trend highlighted by Sutherland and Guedes Soares [5]. In this case, the onset of fibre damage would occur for $U\sim0.16U_p$ earlier than CFRP laminates but later than glass fibre ones. Recalling what asserted in the "Absorbed energy" paragraph, it

is interesting to note the very big distance between the dashed and the continuous line denoting a bigger amount of energy stored elastically, amount that seems to increase at the increasing of the impact energy.

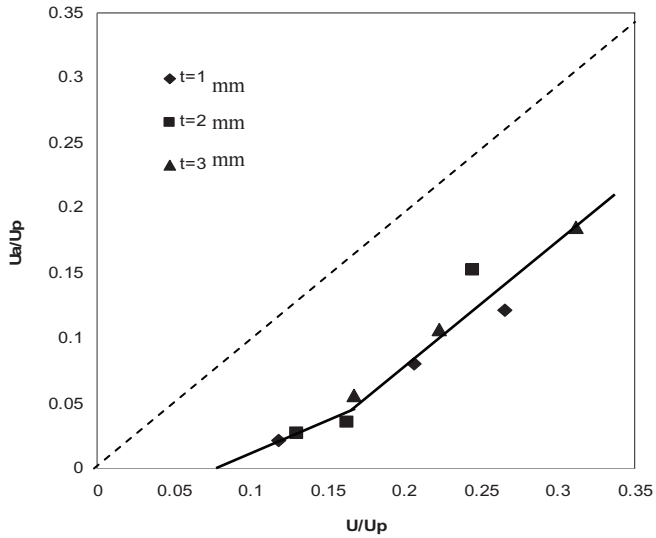

Fig.13. Non dimensional absorbed energy, U_a/U_p, against non dimensional impact energy, U/U_p. Material: BFRP. Mean values.

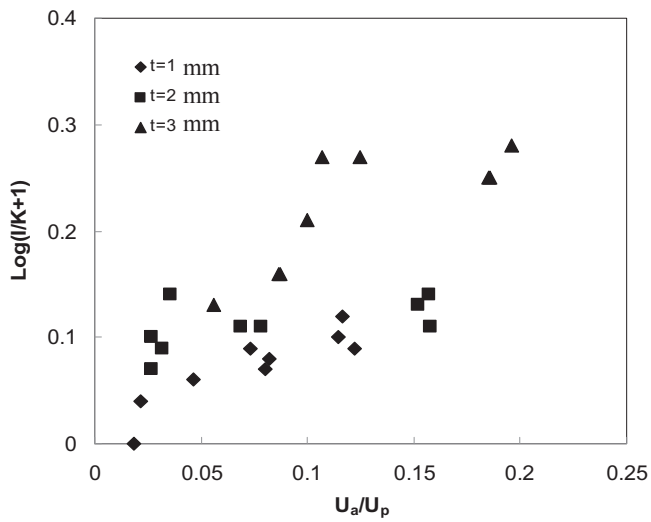

Fig. 14. Diagram for the assessment of the indentation model. Material: BFRP.

The different behaviour respect to the classical laminates could mean a different mechanism of damage confirmed hereafter by the lower indentation values. Of course the assertion needs to be validated by a bigger number of experimental points.

Similarly to Fig. 7 and Fig. 10, Fig. 14 shows the Log(I/k+1) as a function of the non dimensional energy U_a/U_p for BFRP. The k value was varied but in any case the superposition of the points associated with different thicknesses was found not so good. Of course, the poor available data has to take into account so that the discussion will be put off. Also the dependence from the non dimensional absorbed energy reported in fig. 16 seems to be not unique as it happens for classical laminates.

However, plotting I as a function of the absorbed energy U_a (Fig. 15) the data are quite gathered along a single trend irrespective of the thickness.

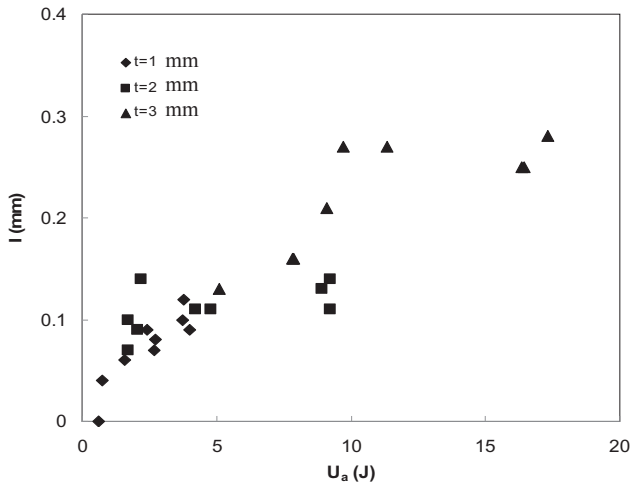

Fig. 15. Indentation, I, against absorbed energy, U_a. Material: BFRP.

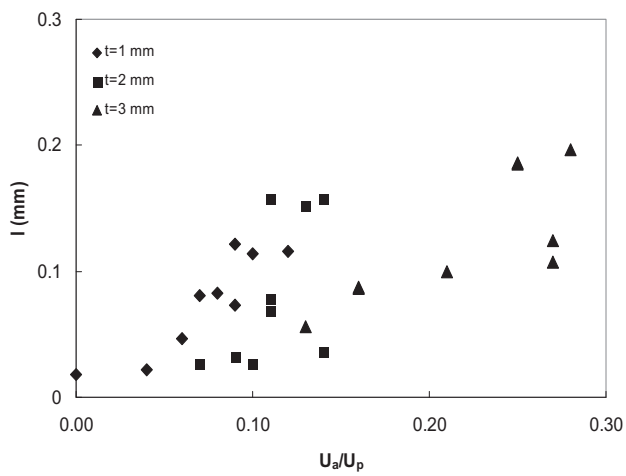

Fig. 16. Indentation, I, against non dimensional absorbed energy, U_a/U_p. Material: BFRP.

Moreover, comparing the I data (Figs. 8, 11 and 16) taking into account the different axis values, lower indentations were found for BFRP laminates. It denotes, as anticipated, a different behaviour: when the same indentation is measured on the three material systems, the basalt fibre laminates absorb a higher portion of energy, if the perforation energy is assumed as a benchmark.

5. Conclusions

In this work, low-velocity impact tests were performed on GFRP and BFRP panels of various thicknesses, varying the initial energy. The scope was the assessment of a simple model to correlate the indentation depth and the absorbed energy. From the results obtained, the main conclusions are as follows:

- at sufficiently high impact energy, the relationship between initial energy and absorbed energy can be reduced to a simple, linear law, independent of the laminate thickness and impactor diameter;
- for GFRP laminates, by an indentation measurement, the absorbed energy can be predicted, provided the perforation energy is known, together with two parameters to be experimentally determined;
- the two parameters appearing in the model are unaffected by the panel thickness and tup diameter; their dependence on the projectile shape and constraint conditions is matter of further research;
- a different behaviour was evidenced by BFRP denoting a different damage mechanism;
- the comparison of the GFRP and BFRP results obtained within this work with similar data previously generated on CFRP laminates, treated according to the proposed model, reveals some differences in the three materials, with reference to the energy absorbed in correspondence of a given dent depth.

References

[1] Dorey G. An overview of impact damage in composites. Inst. Phys. Conf. Series 1989; 102: 395-02.

[2] David-West OS, Nash DH, Banks WM. An experimental study of damage accumulation in balanced CFRP laminates due to repeated impact. Compos. Struct 2008; 83: 247-58.

[3] Richardson MOW, Wisheart MJ. Review of low-velocity impact properties of composite materials. Composites Part A 1996; 27: 1123-31.

[4] Parvatareddy H , Wilson Tsang PH, Dillard DA. Impact damage resistance and tolerance of high-performance polymeric composites subjected to environmental aging. Compos. Sci. Technol 1996; 56: 1129-40.

[5] Sutherland LS, Guedes Soares C. Impact of low fibre-volume, glass/polyester rectangular plates. Compos. Struct 2005; 68: 13-22.

[6] Delfosse D, Poursartip A. Energy-based approach to impact damage in CFRP laminates. Composites Part A 1997; 28A: 647-55.

[7] Caprino G, Langella A, Lopresto V. Indentation and penetration of carbon fibre reinforced plastic laminates. Composites Part B 2003; 34: 319-25.

[8] Lopresto V, Leone C, De Iorio I. Mechanical characterization of basalt fibre reinforced plastic. ETDCM9- 9th International Seminar on Experimental Techniques and Design in Composite Materials 2009 University of Padova– Vicenza (Italy) in press on Compos. Part B.

[9] Caprino G, Iaccarino P, Lopresto V. On the first failure energy of glass-fibre reinforced plastic panels impacted at low-velocity. In press on Composites Part A.

[10] Caprino G, Lopresto V, Scarponi C, Briotti G. Influence of material thickness on the response of graphite fabric/epoxy panels to low velocity impact. Compos. Sci. Technol 1999; 59: 2279-86.